2021 43rd Annual International Conference of the
IEEE Engineering in Medicine & Biology Society (EMBC)
Oct 31 - Nov 4, 2021. Virtual Conference

# Evaluation of Mesh and Sensor Resolution for Finite Element Modeling of Non-Invasive Fetal ECG Signals

Emerson Keenan[1,3], Chandan Karmakar[1,2], Fiona C. Brownfoot[3], and Marimuthu Palaniswami[1]

***Abstract*— Non-invasive fetal electrocardiography (NI-FECG) is an emerging tool with novel diagnostic potential for monitoring fetal wellbeing using electrical signals acquired from the maternal abdomen. However, variations in the geometric structure and conductivity of maternal-fetal tissues have been shown to affect the reliability of NI-FECG signals. Previous studies have utilized detailed finite element models to simulate these impacts, however this approach is computationally expensive. In this study, we investigate a range of mesh and sensor resolutions to determine an optimal trade-off between computational cost and modeling accuracy for simulating NI-FECG signals. Our results demonstrate that an optimal refinement of mesh resolution provides comparable accuracy to a detailed reference solution while requiring approximately 12 times less computation time and one-third of the memory usage. Furthermore, positioning simulated sensors at a 20 mm grid spacing provides a sufficient representation of abdominal surface potentials. These findings represent default parameters to be used in future simulations of NI-FECG signals. Code for the model utilized in this work is available under an open-source GPL license as part of the *fecgsyn* toolbox.**

***Clinical Relevance*— Simulating NI-FECG signals provides the opportunity to study the effects of sensor placement and maternal-fetal anatomic variations in a controlled setting. This work has relevance in determining default parameters for efficiently performing these simulations.**

## I. INTRODUCTION

Non-invasive fetal electrocardiography (NI-FECG) is an emerging tool for monitoring fetal wellbeing using electrical signals acquired from the maternal abdomen [1]. Similar to the adult electrocardiogram, high quality NI-FECG signals can be used for the diagnosis of fetal disorders including cardiac abnormalities, arrhythmias and hypoxia [2], [3].

While NI-FECG holds significant promise as a clinical tool, retrieving a reliable fetal ECG from abdominal recordings is challenging due to the complex conductive medium through which fetal cardiac signals are propagated [4], [5]. To model the impacts of this medium, we recently developed an open-source process which enables simulation of NI-FECG signals in an anatomically accurate geometry [6], [7].

However, simulating the effects of anatomic variations on NI-FECG signals is currently computationally expensive due to the use of high resolution finite element meshes. To compare simulations across a wide range of anatomic configurations, it is critical to optimize the computational cost of this modeling process. This computational cost is primarily determined by two parameters: 1) the number of sensor positions to be simulated, and 2) the resolution and structure of the finite element mesh. Regarding the ideal number of sensor positions, this parameter should be determined by the generated signal characteristics, where sensor positions which generate highly correlated data should be minimized. Regarding the mesh resolution, an optimized finite element mesh should provide substantially similar results to a higher resolution model, at a smaller computational cost.

Previous studies have investigated optimal parameters for finite element mesh generation processes in applications including electroencephalography (EEG) [8] and biomechanical analysis [9]. However, such studies have not been applied to determine optimal parameters in the domain of maternal-fetal electrophysiology.

The aim of this study is to determine an efficient sensor and mesh resolution for simulating NI-FECG signals in an anatomically accurate maternal-fetal geometry. Quantifying the default parameters for this process will enable future simulations to rapidly study a wide range of anatomic variations and ensure our open-source process (available as part of the *fecgsyn* toolbox [2], [10] at www.fecgsyn.com) is computationally accessible to other researchers.

## II. METHOD

To evaluate the effect of varying sensor and mesh resolution on simulated NI-FECG signals, we utilize our previously developed NI-FECG signal model as the basis of this study [6], [7]. This model consists of two core components: 1) the source model representing the fetal cardiac electrical activity and 2) the volume conductor model representing the geometric and conductive properties of the maternal-fetal anatomy.

### A. Source Model

To describe the electrical activation of the fetal heart, we utilize the point dipole model proposed by Sameni et al. [11] which models the fetal cardiac activity as a time-varying $3\times1$ vector $\boldsymbol{d}(t)$ as follows:

$$\boldsymbol{d}(t) = a(t)\hat{x} + b(t)\hat{y} + c(t)\hat{z} \tag{1}$$

where $\hat{x}, \hat{y}, \hat{z}$ are unit vectors along the coordinate axes of the maternal abdomen and $a(t), b(t), c(t)$ are time-varying functions tracing out the path of the cardiac activity.

[1]Department of Electrical and Electronic Engineering, The University of Melbourne, Melbourne, VIC 3010, Australia.
[2]School of Information Technology, Deakin University, Geelong, VIC 3220, Australia.
[3]Department of Obstetrics and Gynaecology, The University of Melbourne, Heidelberg, VIC 3084, Australia.
Correspondence email: e.keenan@ieee.org

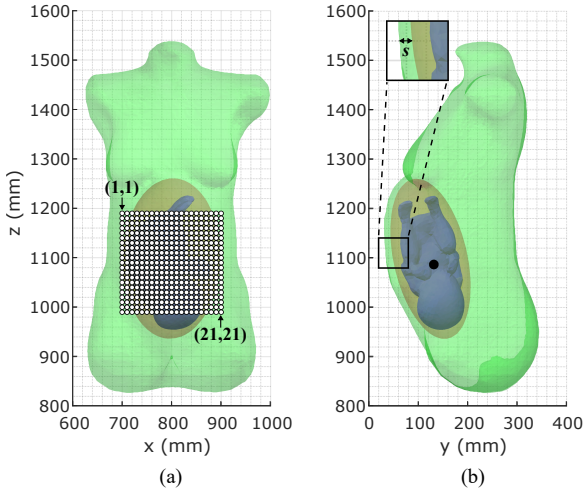


Fig. 1. Overview of model configuration showing (a) 441 sensor positions (○) at a 10 mm grid spacing with sensor positions (1,1) and (21,21) labeled, and (b) fetal cardiac source position (●) and 8 mm separation distance ($s$) between the amniotic fluid and maternal abdomen compartments.

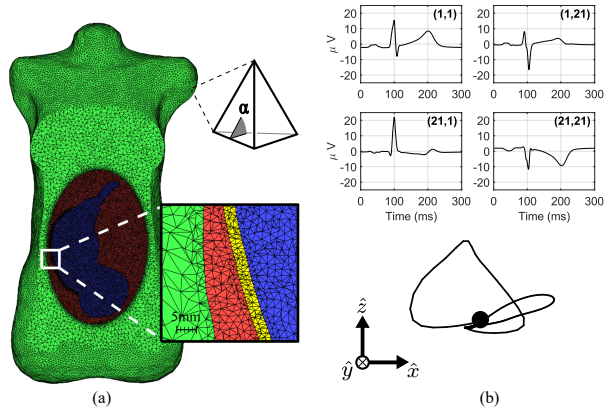


Fig. 2. Visualisation of (a) reference finite element model showing tetrahedral elements with example dihedral angle $\alpha$ and tissue types including fetal body (■), vernix caseosa (■), amniotic fluid (■) and maternal abdomen (■) compartments, and (b) source model orientation with respect to the maternal body axes and examples of simulated NI-FECG signals at four sensor positions using the reference finite element model.

### B. Volume Conductor

The volume conductor model is composed of four compartments consisting of the fetal body, vernix caseosa, amniotic fluid and the maternal abdomen as per our previous work [6], [7]. This model is derived from the Fetus and Mother Numerical Models (FEMONUM) created by Bibin et al. [12], Dahdouh et al. [13] and Daz 3D Studio (www.daz3d.com) based on high resolution MRI and 3D ultrasound data.

To generate NI-FECG signals using this model, we compute a leadfield for each investigated finite element mesh, which represents the linear projection of the source model at $n$ sensor positions in the form $\boldsymbol{\phi}(t) = \boldsymbol{H} \cdot \boldsymbol{d}(t)$, where $\boldsymbol{H}$ represents the $n \times 3$ leadfield matrix, $\boldsymbol{d}(t)$ represents the $3 \times 1$ source model and $\boldsymbol{\phi}(t)$ represents the $n \times 1$ electric potentials at each sensor position.

For this work, we generate a $21 \times 21$ grid of sensors ($n = 441$) positioned at a 10 mm grid spacing, centered over the maternal umbilicus as shown in Fig. 1. The fetal model is placed such that a minimum 8 mm separation is present between the maternal abdominal wall and amniotic fluid to match the minimum thickness observed in clinical studies [14], with a 3 mm layer of vernix caseosa in the back region of the fetal body. The electrical conductivities used for each tissue type in our model are as follows: fetal body ($0.5\ S\ m^{-1}$), vernix caseosa ($10^{-5}\ S\ m^{-1}$), amniotic fluid ($1.6\ S\ m^{-1}$), and maternal abdomen ($0.2\ S\ m^{-1}$) [15].

### C. Mesh Resolution

To determine an optimal finite element mesh, we will vary a set of parameters in the TetGen tool [16] utilized for generating the tetrahedral finite element mesh from the four compartment surfaces in our model. These parameters include the maximum tetrahedral element volume in each compartment, and the target minimum and maximum dihedral angle of each generated tetrahedron. These parameters have been selected for study as they have been shown to affect mesh solution quality [17], [18] and computational cost [8], [19].

Based on our prior work [6], a maximum tetrahedral element volume of 2 mm$^3$, 0.5 mm$^3$, 2 mm$^3$ and 128 mm$^3$ in the fetal body, vernix caseosa, amniotic fluid and maternal abdomen compartments with minimum and maximum dihedral angles of 0 and 165 degrees respectively were used as the reference solution. A visualisation of the reference finite element model and examples of simulated NI-FECG signals using the chosen sensor grid are shown in Fig. 2.

To determine the optimal mesh parameters, we generate a series of leadfields by increasing the maximum tetrahedral volume in each compartment by multipliers of 2, 4, 8, 16, and searching a grid space of 0, 5, 10 degrees for the minimum dihedral angle and 145, 155, 165 degrees for the maximum dihedral angle. Using the results of this process, we calculate the computational cost of each parameterization and compare the leadfield difference between the optimized and reference solutions.

### D. Sensor Resolution

To determine the optimal sensor resolution, we generate a 300 ms fetal dipole signal using the source parameters given in Table 2 of [6] and compare the correlation of signals generated at each sensor position to signals generated at a displacement $x$ mm to the left, right, above and below each sensor position, where $x$ is set at a value of 10 mm, 20 mm or 30 mm. This process aims to determine the smallest number of sensors which provide a sufficient representation of NI-FECG potentials. A high correlation between sensors indicates they are generating redundant information at added computational expense, while a low correlation indicates that large NI-FECG signal changes are occurring between sensor positions. For this analysis, we use the leadfield computed using the reference finite element model and compare the mean correlation at each sensor position.

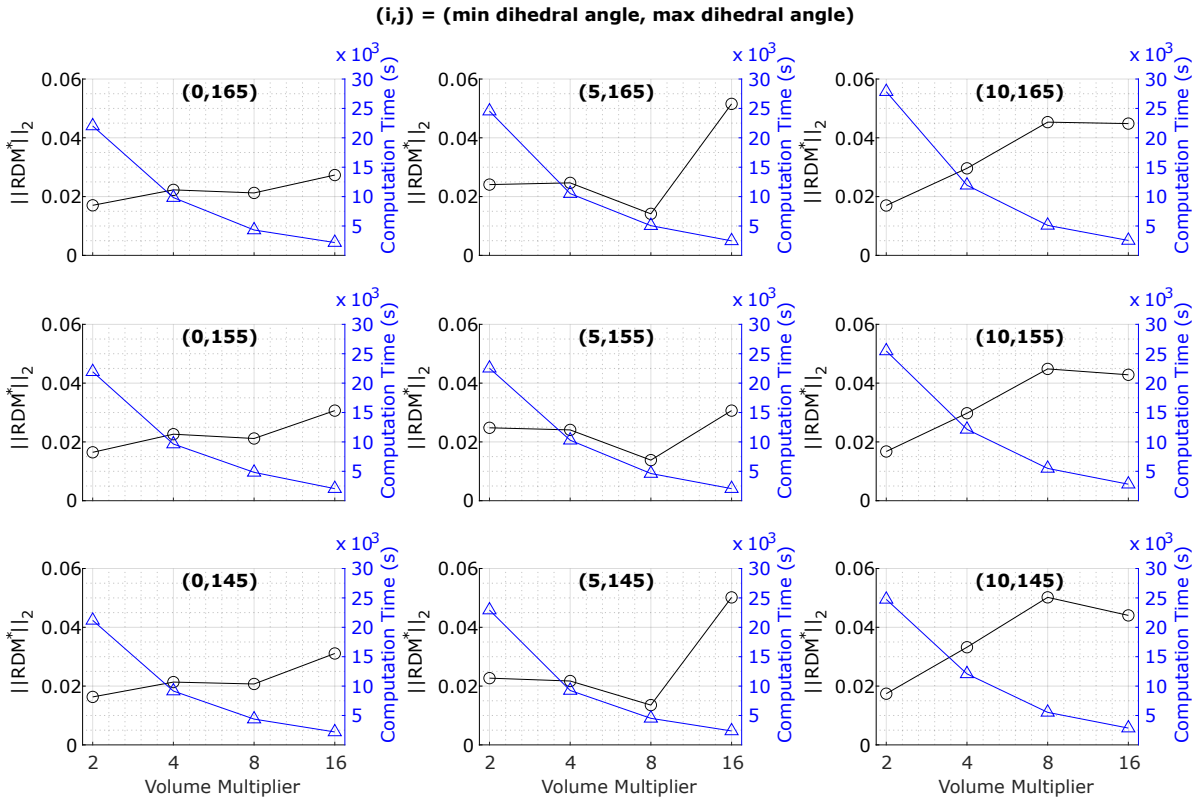


Fig. 3. Model optimization results where each panel indicates $\|RDM^*\|_2$ error (—○—) of the optimized leadfield solution compared to the reference solution and computation time (—△—) for different combinations of the mesh refinement parameters: minimum dihedral angle, maximum dihedral angle and volume multiplier. For each investigated model, the maximum tetrahedral volume in each compartment was multiplied by the volume multiplier given on the x axis.

### *E. Metrics*

To compare leadfield solutions for each model, we utilize the relative difference measure ($RDM^*$) proposed by Meijs et al. [20].

$$RDM^* = \left\| \frac{x_a}{\|x_a\|_2} - \frac{x_b}{\|x_b\|_2} \right\|_2 \tag{2}$$

where $x_a$ and $x_b$ are $n \times 1$ vectors for inputs $a$ and $b$ respectively. Each $x_a$ or $x_b$ represents a column of the respective leadfield matrix, equivalent to the electric potential produced by a unit dipole along the x, y or z axis. Thus, $RDM^*$ indicates the difference in distribution patterns of electric potentials, bounded by 0 for identical inputs and 2 for $x_a = -x_b$. To provide a single metric for comparison, we calculate $\|RDM^*\|_2$ as the 2-norm of $RDM^*$ values computed for each column of the optimized leadfield solution compared to the reference leadfield solution. For this work, an $\|RDM^*\|_2$ of less than 0.02 is considered accurate [6].

To compare signals generated using the reference model at different sensor positions, we utilize the Pearson correlation coefficient. Computational cost is quantified as the total computation time and peak physical memory usage during mesh generation and leadfield solution.

## III. RESULTS AND DISCUSSION

All simulations were performed in MATLAB 2019b (MathWorks, USA) on the University of Melbourne's High Performance Computing system [21]. Each simulation was performed on a single virtual machine with a four-core 2.3 Ghz Intel Xeon E5 CPU and 16 GB RAM to approximate a modern workstation specification.

### *A. Mesh Resolution*

As can be seen in Fig. 3, increasing the volume multiplier generally trends towards larger $\|RDM^*\|_2$ values for all investigated parameters, with the exception of solutions utilizing a minimum dihedral angle of 5 degrees. In this case, it can be seen that a minimum overall $\|RDM^*\|_2$ of 0.014 is achieved for a volume multiplier of 8 with a maximum dihedral angle of 145 degrees. The relationship between the minimum and maximum dihedral angle can also be seen to affect the general shape of the error trend, where increasing the minimum dihedral to 10 degrees results in overall worse performance compared to an angle of 0 degrees.

Regarding the computation time, varying the tetrahedral element volume has the largest effect, where increasing the volume multiplier decreases computation time non-linearly. The next largest effect on computation time can be attributed to the minimum dihedral angle where increasing the minimum dihedral angle results in increased computation times.

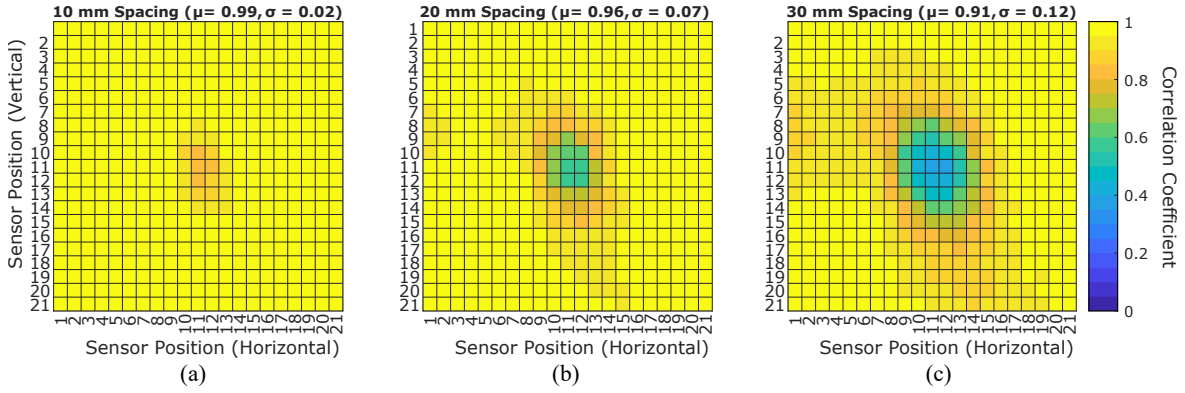


Fig. 4. Heatmaps showing correlation coefficient of signals at each sensor position compared to signals at a spacing of (a) 10 mm, (b) 20 mm, and (c) 30 mm. For each spacing, mean ($\mu$) and standard deviation ($\sigma$) of the correlation coefficient across all sensor positions is shown in the plot title.

From Fig. 3, it can be seen that the lowest computation time achieved by a model with an $\|RDM^*\|_2$ under 0.02 is produced by the configuration described in Table I. This configuration results in comparable accuracy to the reference solution while requiring approximately 12 times less computation time and one-third of the peak physical memory usage.

It should be noted that the generalization of these results may depend on the particular configuration of the maternal-fetal anatomy studied. Changes such as significantly modifying the separation distance between compartments, tissue conductivities or dipole position requires further analysis to ensure comparable accuracy [22].

### B. Sensor Resolution

In terms of sensor resolution, it can be seen in Fig. 4 that a sensor spacing of 10 mm generates highly correlated results at every sensor position ($\mu = 0.99, \sigma = 0.02$), indicating that a large amount of redundant sensor data is being generated. As the sensor spacing increases, it can be seen that this correlation is reduced at a spacing of 20 mm ($\mu = 0.96, \sigma = 0.07$) and 30 mm ($\mu = 0.91, \sigma = 0.12$).

Based on these results, it is recommended in future simulations that a sensor spacing of 20 mm is used to provide a sufficient representation of abdominal potentials without unnecessarily increasing computational cost.

It is important to observe that the utilised correlation metric does not specifically assess differences in ECG features such as the T wave or QRS complex amplitude. Further study should be performed to determine changes in ECG features across different sensor spacings.

## IV. CONCLUSION

In this study, we determined an efficient set of sensor and mesh resolution parameters for simulating NI-FECG signals in an anatomically accurate maternal-fetal geometry. These parameters will enable future simulations to rapidly study a wide range of anatomic variations in a computationally accessible manner. Code for the utilized model is available under an open-source GNU GPL license as part of the *fecgsyn* toolbox (available at www.fecgsyn.com).

TABLE I

COMPUTATIONAL COST OF OPTIMIZED MODEL COMPARED TO REFERENCE SOLUTION FOR 441 SENSOR POSITIONS SHOWN IN FIG. 1

| | Parameter Names † | Parameter Values | Computation Time (s) | Peak Physical Memory Usage (MB) |
|---|---|---|---|---|
| *Reference* | $V_f$ | 2 mm$^3$ | 54685 | 6560 |
| | $V_v$ | 0.5 mm$^3$ | | |
| | $V_a$ | 2 mm$^3$ | | |
| | $V_m$ | 128 mm$^3$ | | |
| | $D_{min}$ | 0 | | |
| | $D_{max}$ | 165 | | |
| *Optimized* | $V_f$ | 16 mm$^3$ | 4517 | 2136 |
| | $V_v$ | 4 mm$^3$ | | |
| | $V_a$ | 16 mm$^3$ | | |
| | $V_m$ | 1024 mm$^3$ | | |
| | $D_{min}$ | 5 | | |
| | $D_{max}$ | 145 | | |
| **Optimized vs Reference Improvement** | | | 12.1× | 3.1× |

† parameters are as follows: $V_f$ = maximum fetal body tetrahedral element volume, $V_v$ = maximum vernix caseosa tetrahedral element volume, $V_a$ = maximum amniotic fluid tetrahedral element volume, $V_m$ = maximum maternal abdomen tetrahedral element volume, $D_{min}$ = minimum dihedral angle, $D_{max}$ = maximum dihedral angle.


## ACKNOWLEDGMENT

Emerson Keenan is supported by an Australian Government Research Training Program Scholarship at the University of Melbourne. Fiona Brownfoot is supported by a NHMRC Early Career Fellowship (NHMRC #1142636) and a Norman Beischer Clinical Research Fellowship.


## REFERENCES


[1] G. D. Clifford *et al.*, "Non-invasive fetal ECG analysis," *Physiological Measurement*, vol. 35, no. 8, p. 1521, 2014.

[2] F. Andreotti *et al.*, "An open-source framework for stress-testing non-invasive foetal ECG extraction algorithms," *Physiological Measurement*, vol. 37, no. 5, p. 627, 2016.

[3] E. Keenan *et al.*, "Entropy Profiling for Detection of Fetal Arrhythmias in Short Length Fetal Heart Rate Recordings," in *2020 42nd Annual International Conference of the IEEE Engineering in Medicine Biology Society (EMBC)*, Jul. 2020, pp. 621–624.
[4] T. F. Oostendorp *et al.*, "The effect of changes in the conductive medium on the fetal ECG throughout gestation," *Clinical Physics and Physiological Measurement*, vol. 10, no. 4B, p. 11, 1989.
[5] E. Keenan *et al.*, "The Influence of Vectorcardiogram Orientation on the T/QRS Ratio Obtained Via Non-Invasive Fetal ECG," in *2019 41st Annual International Conference of the IEEE Engineering in Medicine and Biology Society (EMBC)*, Jul. 2019, pp. 1883–1886.
[6] E. Keenan *et al.*, "The effects of asymmetric volume conductor modeling on non-invasive fetal ECG extraction," *Physiological Measurement*, vol. 39, no. 10, p. 105013, 2018.
[7] E. Keenan *et al.*, "Personalized Anatomic Modeling for Noninvasive Fetal ECG: Methodology and Applications," *IEEE Transactions on Instrumentation and Measurement*, vol. 70, pp. 1–12, 2021.
[8] S. Lew *et al.*, "Accuracy and run-time comparison for different potential approaches and iterative solvers in finite element method based EEG source analysis," *Applied Numerical Mathematics*, vol. 59, no. 8, pp. 1970–1988, Aug. 2009.
[9] J. A. Bright and E. J. Rayfield, "The Response of Cranial Biomechanical Finite Element Models to Variations in Mesh Density," *The Anatomical Record*, vol. 294, no. 4, pp. 610–620, 2011.
[10] J. Behar *et al.*, "An ECG simulator for generating maternal-foetal activity mixtures on abdominal ECG recordings," *Physiological Measurement*, vol. 35, no. 8, p. 1537, 2014.
[11] R. Sameni *et al.*, "Multichannel ECG and Noise Modeling: Application to Maternal and Fetal ECG Signals," *EURASIP Journal on Advances in Signal Processing*, vol. 2007, no. 1, p. 043407, Dec. 2007.
[12] L. Bibin *et al.*, "Whole-body pregnant woman modeling by digital geometry processing with detailed uterofetal unit based on medical images," *IEEE Transactions on Biomedical Engineering*, vol. 57, no. 10, pp. 2346–2358, Oct. 2010.
[13] S. Dahdouh *et al.*, "A comprehensive tool for image-based generation of fetus and pregnant women mesh models for numerical dosimetry studies," *Physics in Medicine and Biology*, vol. 59, no. 16, p. 4583, 2014.
[14] J. Kim *et al.*, "Thickness of Rectus Abdominis Muscle and Abdominal Subcutaneous Fat Tissue in Adult Women: Correlation with Age, Pregnancy, Laparotomy, and Body Mass Index," *Archives of Plastic Surgery*, vol. 39, no. 5, pp. 528–533, Sep. 2012.
[15] J. G. Stinstra and M. J. Peters, "The Influence of Fetoabdominal Tissues on Fetal ECGs and MCGs," *Archives of Physiology and Biochemistry*, vol. 110, no. 3, pp. 165–176, Jan. 2002.
[16] H. Si, "TetGen, a Delaunay-Based Quality Tetrahedral Mesh Generator," *ACM Trans. Math. Softw.*, vol. 41, no. 2, pp. 11:1–11:36, Feb. 2015.
[17] M. Kŕížek, "On the Maximum Angle Condition for Linear Tetrahedral Elements," *SIAM Journal on Numerical Analysis*, vol. 29, no. 2, pp. 513–520, Apr. 1992.
[18] J. R. Shewchuk, "What is a Good Linear Element? - Interpolation, Conditioning, and Quality Measures," in *In 11th International Meshing Roundtable*, 2002, pp. 115–126.
[19] E. Bellenger and P. Coorevits, "Adaptive mesh refinement for the control of cost and quality in finite element analysis," *Finite Elements in Analysis and Design*, vol. 41, no. 15, pp. 1413–1440, Sep. 2005.
[20] J. W. H. Meijs *et al.*, "On the numerical accuracy of the boundary element method," *IEEE Transactions on Biomedical Engineering*, vol. 36, no. 10, pp. 1038–1049, Oct. 1989.
[21] B. Meade *et al.*, "Spartan HPC-Cloud Hybrid: Delivering Performance and Flexibility," Apr. 2017. [Online]. Available: https://doi.org/10.4225/49/58ead90dceaaa
[22] J. Vorwerk, "New finite element methods to solve the EEG/MEG forward problem," PhD Thesis, Westfälische Wilhelms-Universität Münster, 2016.